



# Wet-to-dry shift over Southwest China in 1994 tied to the warming of tropical warm pool

Lin Wang<sup>1</sup> · Gang Huang<sup>2</sup> · Wen Chen<sup>2,3</sup> · Wen Zhou<sup>4</sup> · Weiqiang Wang<sup>5</sup>

Received: 3 September 2017 / Accepted: 3 January 2018 / Published online: 10 January 2018  
© Springer-Verlag GmbH Germany, part of Springer Nature 2018

## Abstract

The autumn climate in Southwest China (SWC) experienced a notable wet-to-dry shift in 1994. Associated with this change in precipitation, decadal signatures of large-scale atmospheric circulation and SST identify a likely dynamical origin: the tropical warm pool (TWP) consisting of tropical northwest Pacific (TNWP, 3°S–12°N and 110°E–150°E) sector and tropical east Indian Ocean (TEI, 10°S–3°N and 80°E–110°E) sector. A cold-to-warm phase switch of TWP SST occurred in 1994, coinciding exactly with the timing of the regime transition of SWC precipitation. During post-1994 period, warm states in the TNWP and TEI sectors plays in a synergistic fashion to invoke dry decades in SWC. On the one side, warm SST over the TNWP sector excites an anomalous cyclone centered on the South China Sea directed opposite to the climatological moisture transport and strengthened zonal wind to its west accompanied by a weakening of the poleward flux; on the other side, warm SST over the TEI sector acts to intensify inflow into TEI with less concurrent transfer of moisture to SWC and to steer moisture to the northern Arabic Sea and away from the SWC-oriented track. Meanwhile, the troposphere over SWC is capped by subsidence, which is jointly contributed by TNWP and TEI. It then follows a reduced moisture supply, suppressed convective activity, and anomalous divergence in SWC, bringing a precipitation deficit there. In contrast, cold TWP SST during 1961–1994 favors wet conditions in SWC, given a perfectly symmetrical circulation pattern. Further, the dominant role of TWP is confirmed, because the modeled response to TWP SST forcing alone bears a great resemblance to the observed evidence. Finally, it is also found that the teleconnected influence induced by TWP is stronger in southern SWC than in northern SWC, which explains the south-north gradient of interdecadal signal of SWC precipitation.

**Keywords** Drought · Southwest China · Decadal shift · Tropical warm pool · SST

## 1 Introduction

In recent decades, there have been recurring disastrous droughts in Southwest China (SWC), with the summer of 2006 (Peng et al. 2007), the autumn of 2009 to the spring of 2010 (Huang et al. 2012), the late summer of 2011 (Wang et al. 2012), and the spring of 2013 (Duan et al. 2014) being the record-breaking events during the last 50 years. These drought events have resulted in tremendous losses, including crop failure, a lack of drinking water, ecosystem destruction, health problems, and even deaths (Wang et al. 2015a). The first wave of droughts swept across SWC during the summer of 2006, causing drinking water shortages to at least 18 million people and an economic loss of 11.74 billion yuan (the official currency in China). During the long-lasting drought from autumn 2009 to the ensuing spring of 2010, more than 16 million residents and 11 million livestock suffered

✉ Gang Huang  
hg@mail.iap.ac.cn

<sup>1</sup> CAS Key Laboratory of Regional Climate-Environment for Temperate East Asia, Institute of Atmospheric Physics, Chinese Academy of Sciences, Beijing 100029, China

<sup>2</sup> State Key Laboratory of Numerical Modeling for Atmospheric Sciences and Geophysical Fluid Dynamics, Institute of Atmospheric Physics, Chinese Academy of Sciences, P.O. Box 9804, Beijing 100029, China

<sup>3</sup> Center for Monsoon System Research, Institute of Atmospheric Physics, Chinese Academy of Sciences, Beijing 100190, China

<sup>4</sup> Guy Carpenter Asia-Pacific Climate Impact Centre, School of Energy and Environment, City University of Hong Kong, Hong Kong, China

<sup>5</sup> State Key Laboratory of Tropical Oceanography, South China Sea Institute of Oceanology, Chinese Academy of Sciences, Guangzhou, China

from water shortages, and direct economic losses were estimated at 19 billion yuan. Only one year later, SWC was again greatly affected by drought, with a total of 5.86 million hectares of crop failures and water shortages for 12 million people and 9.17 million livestock. Before the affected regions were able to recover adequately, another drought began to form during the autumn of 2012 and reached peak intensity in the spring of 2013, when nearly 29.38 million people were at risk and 4.35 million needed urgent life-saving aid.

Prior to this series of droughts occurring over SWC, there had been intensive focus on drought and flooding across eastern China (e.g. Chen et al. 2009, 2015; Feng et al. 2011, 2014a; Yuan et al. 2012; Jia and Ge 2017). However, SWC droughts during the last decade have attracted great concern from both the Chinese government and the academic sector. To date, considerable efforts have been dedicated to exploring multiple aspects of droughts in SWC, and most of the contributions can be roughly categorized into two groups: one is related to the characteristics of variability and the other to the physical mechanisms responsible (Wang et al. 2015a). On the one hand, it is found that droughts in SWC have become more intense and frequent during the past 50 years (Wang and Chen 2012; Wang et al. 2016; Sun et al. 2016, 2017) and they are projected to continue throughout the twenty-first century (Wang et al. 2014). On the other hand, many studies have attempted to unveil the critical patterns of SST and atmospheric systems that have significant influence on the lack of rainfall in SWC; this progress has been comprehensively reviewed by Wang et al. (2015a). Here, we want to emphasize that most research has been centered on case studies (e.g., Peng et al. 2007; Li et al. 2009; Barriopedro et al. 2012; Huang et al. 2012; Yang et al. 2012) and interannual variability (e.g., Feng et al. 2014b; Wang et al. 2015b; Li and Zhou 2016), but interdecadal variability has not been well addressed so far. As we know, decadal oscillations cause an overall climate background and have a large influence on interannual variability and extremes (e.g., Ding et al. 2008; Zhang et al. 2008; Li et al. 2012; Wu et al. 2012; Chen et al. 2012, 2013; Liu and Sui 2014; Jia et al. 2014, 2015; Piao et al. 2017). More recently, Tan et al. (2017) examined decadal winter drought in SWC and its atmospheric teleconnection; Zhang et al. (2017) revealed the causes of the long-term decrease in summer precipitation over SWC by tracing changes in moisture supply. This study focuses on interdecadal shifts in dryness/wetness over SWC in autumn (September to November), a key season that triggers persistent dry conditions heading into the ensuing winter and spring.

This study is organized as follows. Section 2 describes the data, methods, and numerical models. In Sect. 3, statistical diagnoses and numerical experiments are performed to physically understand the decadal variability of SWC

precipitation and its connection to SST and atmospheric circulation. Finally, concluding remarks and further discussions are given in Sect. 4 and Sect. 5, respectively.

## 2 Data, methods and models

### 2.1 Data

China gridded monthly precipitation dataset with  $0.5^\circ \times 0.5^\circ$  horizontal resolution since 1961 is released and routinely updated by the National Meteorological Information Center (NMIC) of the China Meteorological Administration. This product is built through thin plate spline interpolation of about 2400 rain gauge observations to the nodes of the  $0.5^\circ$  grid, with the digital elevation model GTOPO30 incorporated to eliminate the influence of elevation on precipitation. On the whole, this dataset has proven to be of good quality, since the generation process is subjected to rigorous quality control (NMIC 2012). In parallel, the gridded observed potential evapotranspiration (PET) dataset at monthly intervals is retrieved from the latest version (Harris et al. 2014) of the Climatic Research Unit (CRU). The CRU PET, derived based on a variant of the Penman–Monteith method, accounts for the combined effects of temperature, radiation and humidity. The horizontal grid of the PET dataset provided by CRU coincides with that of the precipitation data prepared by the NMIC.

To examine the SST and atmospheric teleconnection patterns associated with precipitation variability, this study uses Extended Reconstructed Sea Surface Temperature (ERSST) data on a  $2^\circ \times 2^\circ$  grid, developed by NOAA (Smith et al. 2008) and Japanese 55-year Reanalysis (JRA-55) data on a  $1.25^\circ$  latitude–longitude grid at 37 pressure levels, compiled by the Japan Meteorological Agency (Kobayashi et al. 2015; Harada et al. 2016). The variables analyzed include SST, vertically integrated moisture transport, vertical velocity, total precipitable water, and wind vectors.

Note that all of these data are used for the period 1961–2013.

### 2.2 Methods

The breakpoint in time series with interdecadal change is detected from the generalized fluctuation test framework (Kuan and Hornik 1995; Zeileis et al. 2003), which fits a model to the given data and derives an empirical process that captures the fluctuation either in residuals or in parameter estimates. In this study, the empirical fluctuation process is computed based on cumulative sums with ordinary least squares residues (OLS-based CUSUM), as introduced by Ploberger and Krämer (1992). A segment of the CUSUM chart with an upward slope indicates a period when the

values tend to be above the overall average; likewise, a segment with a downward slope indicates a period when the values tend to be below the overall average. Thus, a peak or valley of the CUSUM trajectory that exceeds the confidence threshold corresponds to a sudden shift in the average.

Drought indices are quantitative measures that characterize dry and wet levels by assimilating data from one or several indicators into a single numerical value. Thus, besides precipitation consideration, we also employ two well-known drought indices: Standardized Precipitation Evapotranspiration Index (SPEI) and Standardized Precipitation Index (SPI). The complete calculation procedures of SPEI and SPI are available in Vicente-Serrano et al. (2010). SPEI is an extension of SPI and able to capture impact of evaporation on water demand, while SPI is solely dependent on precipitation. Therefore, the difference between SPEI and SPI illustrates the contribution of evaporation anomalies.

Correlation and composite analyses are performed to diagnose relationships between precipitation and large-scale climate features.

### 2.3 Models

Numerical model simulation is a useful tool for interpreting and isolating detailed physical mechanisms linking SST, circulation, and rainfall. To carry out the investigations, we use two types of numerical models: one is the moist Linear Baroclinic Model (LBM) version 2.2, and the other is the Community Atmospheric Model (CAM) version 5.1. LBM is linearized atmospheric model by removing nonlinearity in the dynamical atmosphere, so that simulated results would be much easily interpreted. Compared to LBM, CAM is a fully nonlinear atmospheric model with a number of physical processes and feedbacks involved, which aims to yield a realistic representation of the climate system.

Moist LBM incorporates interacting moist processes of the convection and surface heat fluxes into the conventional LBM, in order to obtain a steady atmospheric response to a prescribed SST anomaly. It has a spectral T21 horizontal resolution with 20 vertical levels, and utilizes biharmonic thermal diffusion and linear drag which mimics Rayleigh friction and Newtonian damping. The basic state is derived from the autumn (September–November) mean climatology of the ECMWF reanalysis data (ERA40) during 1961–1990. LBM is integrated forward in time to reach equilibrium. Full details of moist LBM can be found in Watanabe and Jin (2003).

CAM is an atmospheric general circulation model (AGCM) and released as the atmospheric component of the Community Earth System Model version (CESM). It is configured to run with the finite volume dynamical core at a horizontal resolution of  $1.9^\circ$  latitude and  $2.5^\circ$  longitude

with 26 levels in the vertical. The relevant information about CAM5.1 can be found in Neale et al. (2012).

## 3 Analysis

### 3.1 Decadal structure of autumn precipitation in SWC

The top panel of Fig. 1 outlines the domain of SWC, which covers an area of approximately  $1.23$  million  $\text{km}^2$ , or  $12.9\%$  of China, with latitude and longitude ranging from  $22^\circ\text{N}$  to  $32^\circ\text{N}$  and  $98^\circ\text{E}$  to  $110^\circ\text{E}$ , respectively. SWC comprises four provinces and one municipality: Sichuan, Guizhou, Yunnan, west of Guangxi, and Chongqing. The precipitation in SWC is characterized by a strong annual cycle with rainy summer and dry winter, as shown in the bottom panel of Fig. 1. Autumn precipitation is  $22\%$  of the annual total, ranking as the second wettest calendar season. Because winter is a climatological dry season, a significant reduction in autumn precipitation will lead to sustained and enhanced drought. Therefore, it is of great significance to discuss autumn

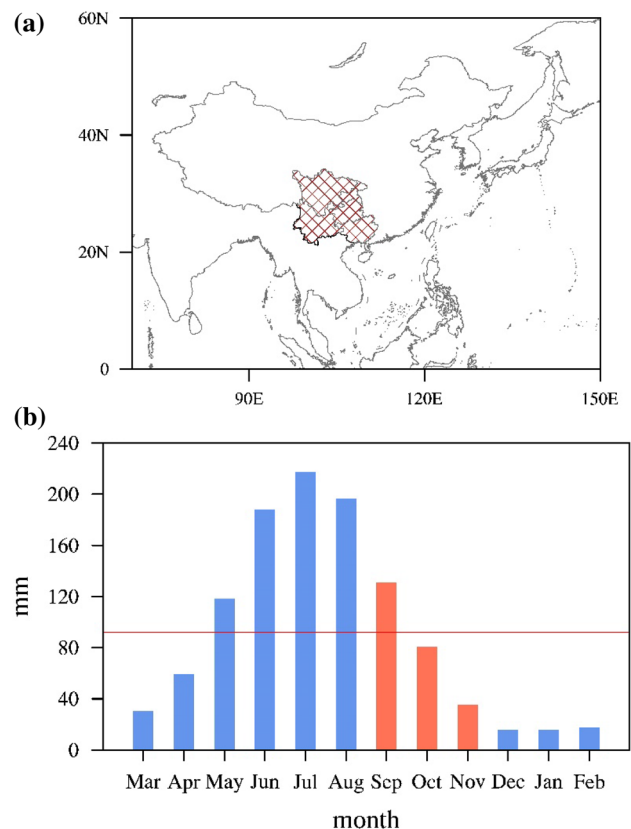


**Fig. 1** **a** Geographic location of SWC (brown cross-hatching). **b** The annual cycle of precipitation for SWC, with the annual mean marked by the horizontal red line

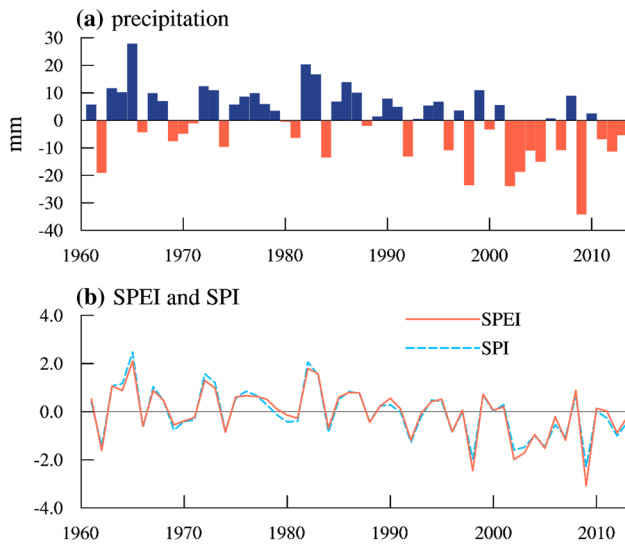


**Fig. 2** Temporal anomalies of autumn precipitation (a), SPEI (b, red solid) and SPI (b, blue dashed) in SWC from 1961 to 2013

drought, although the majority of precipitation falls in the summer.

Figure 2 shows the autumn (September to November) averaged anomalies of precipitation (a), SPEI (b, red line) and SPI (b, blue line) for SWC from 1961 to 2013, with respect to the entire period of record. On the one side, there appears to be virtually no discrepancy between SPEI and SPI, indicating dominant role of precipitation whilst negligible contribution of other factors including temperature, radiation and humidity. On the other side, it reveals a close correspondence between precipitation and drought indices, with correlation coefficient being 0.97. These two points qualify the use of precipitation to identify the characteristics of dry and wet spells in the following discussion.

To determine the decadal regime shift, a CUSUM plot using the OLS residuals is drawn in Fig. 3a. The CUSUM path is bowed, implying that the mean of the series is not stable during the period with one change point. Obviously, the curve goes outside the 5% significance level and takes a sudden turn from climbing to declining in 1994, which indicates that around this time the average shifted from above-average to below-average. Thereby, the OLS-based CUSUM test detects an abrupt shift to drier conditions in 1994, prior to which rainfall is generally above average. Meanwhile, the mutation tests on SPEI and SPI, as expected, lead to the same conclusion. Furthermore, the seven most humid years (1963, 1965, 1972, 1973, 1982, 1983, and 1986) all occurred before 1994, while the decades since 1995 contain the top three driest years (1998, 2002, and 2009).

If we inspect the full period, the precipitation series shows a mathematically decreasing trend with a rate of  $-0.32$  mm per year, which is significant at the 95% confidence level.

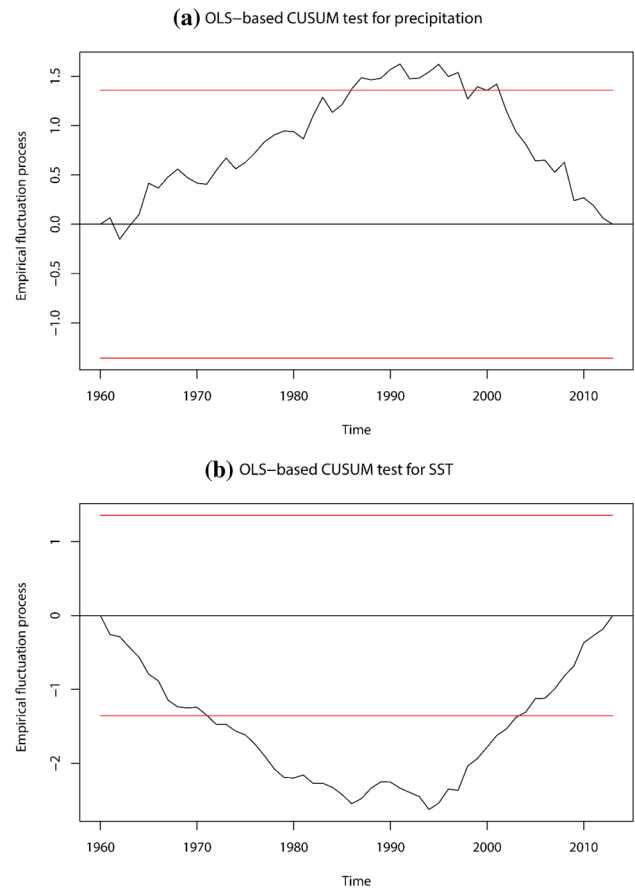


**Fig. 3** OLS-based CUSUM processes (black curve) with 5% significance level (horizontal red line) for SWC precipitation (a) and TWP SST (b)

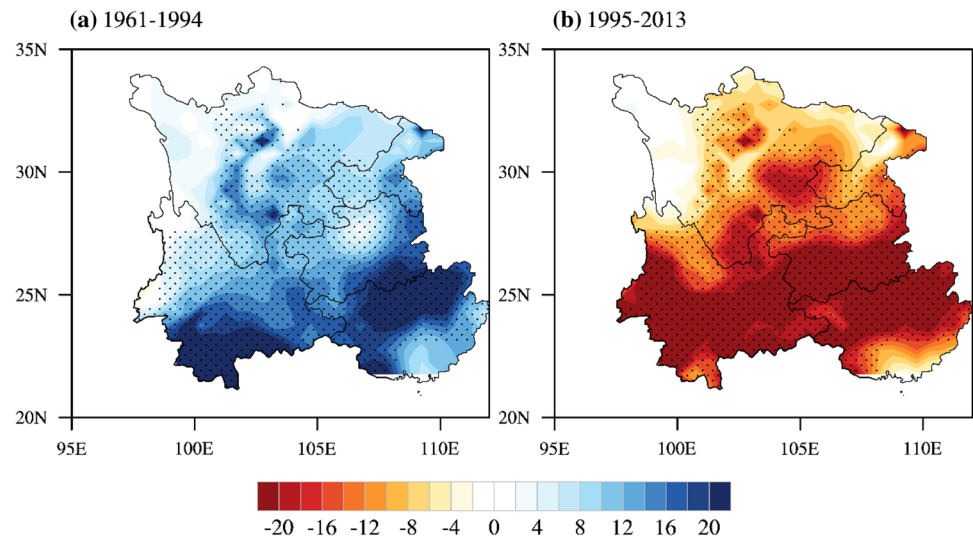
However, the same tests applied for two periods, 1961–1994 and 1995–2013, have  $P$  values of 0.77 and 0.5, respectively, indicating acceptance of the null hypothesis of “no trend” with high probability. Therefore, such changes are more closely tied to decadal climate cycles rather than a continuous tendency toward drier conditions.

Table 1 shows a complete list of the dry and wet years identified with precipitation less or more than half a standard deviation. There is a sharp contrast between the two periods of 1961–1994 and 1995–2013: the earlier period is a wet epoch, with 15 (44%) wet versus 6 (18%) dry cases, while the reverse is true for the more recent period, with a much higher proportion of dry (53%) than wet years (15%). In order to establish the circulation and SST patterns associated with decadal precipitation variability, the composite fields of wet years during 1961–1994 and dry years during 1995–2013 are compared. In addition, the reversal in relative frequencies of dry and wet years is not sensitive to the specific values chosen for the thresholds.

Figure 4 depicts the spatial pattern of the precipitation composite in SWC corresponding to wet and dry decades.

**Table 1** Dry and wet years of over half a standard deviation for two decades (1961–1994 and 1995–2013)

	1961–1994 (34 years)	1995–2013 (19 years)
Dry ( $P < -0.5\sigma$ )	1962, 1969, 1974, 1981, 1984, 1992	1996, 1998, 2002, 2003, 2004, 2005, 2007, 2009, 2011, 2012
Wet ( $P > 0.5\sigma$ )	1963, 1964, 1965, 1967, 1968, 1972, 1973, 1976, 1977, 1982, 1983, 1985, 1986, 1987, 1990	1995, 1999, 2008

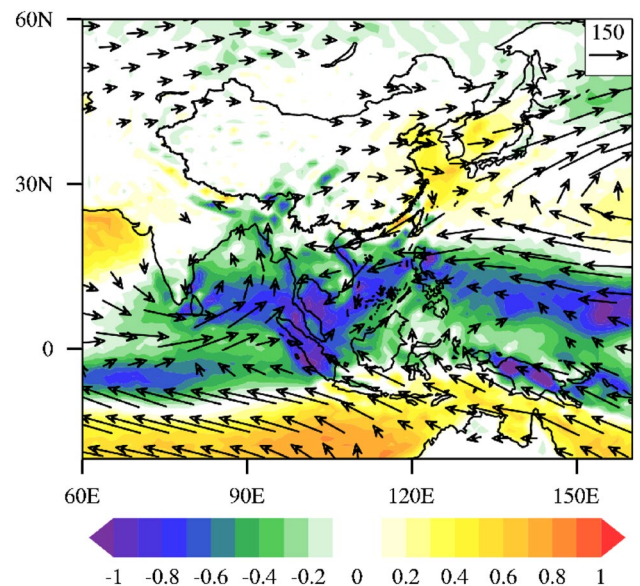
**Fig. 4** Composite maps of autumn precipitation anomalies (shadings, units: mm) in SWC for wet years 1961–1994 (a) and dry years (defined in text) 1995–2013 (b). The stippling indicates negative or positive anomalies greater than the 90% confidence level

During the former decadal period, a broad area of SWC receives more precipitation compared to climatology, while rainfall deficits overwhelm the whole region after the 1994 shift. Quantitative evaluation shows that there is 29% more precipitation (90 versus 70 mm) in the wet period than in the dry period. This figure also suggests that the decadal signal is not geographically homogeneous but varies from above 20 mm in the south to less than 10 mm in the north.

### 3.2 Circulation and SST patterns associated with decadal precipitation variability

The autumn climatology of vertically integrated moisture flux and divergence is shown in Fig. 5, in which two main transport routes of water vapor into SWC are exhibited. One is related to a large-scale anticyclone centered on the South China Sea, which takes moisture across the South China Sea and Indo-China peninsular into SWC. The other is a poleward conveyor stretching from the equatorial Indian Ocean to SWC. These two channels merge into one toward the northeast before entering SWC. Future work will need a quantitative estimate of moisture source contributions based on trajectory tracking model, for example Zhang et al. (2017).

Figure 6 shows large-scale atmospheric circulation patterns associated with decadal fluctuations in SWC precipitation, involving vertically integrated moisture transport and

**Fig. 5** Climatological pattern of vertically integrated moisture flux (vectors, units:  $\text{kg s}^{-1} \text{m}^{-1}$ ) and divergence (shadings, units:  $10^{-4} \text{kg s}^{-1} \text{m}^{-2}$ ) for East Asia. Vectors with magnitudes less than  $50 \text{kg s}^{-1} \text{m}^{-1}$  are masked out

divergence, column precipitable water, vertical velocity at 500 hPa and divergent wind at 200 hPa. In what follows, we describe mainly the composite patterns tied to the dry

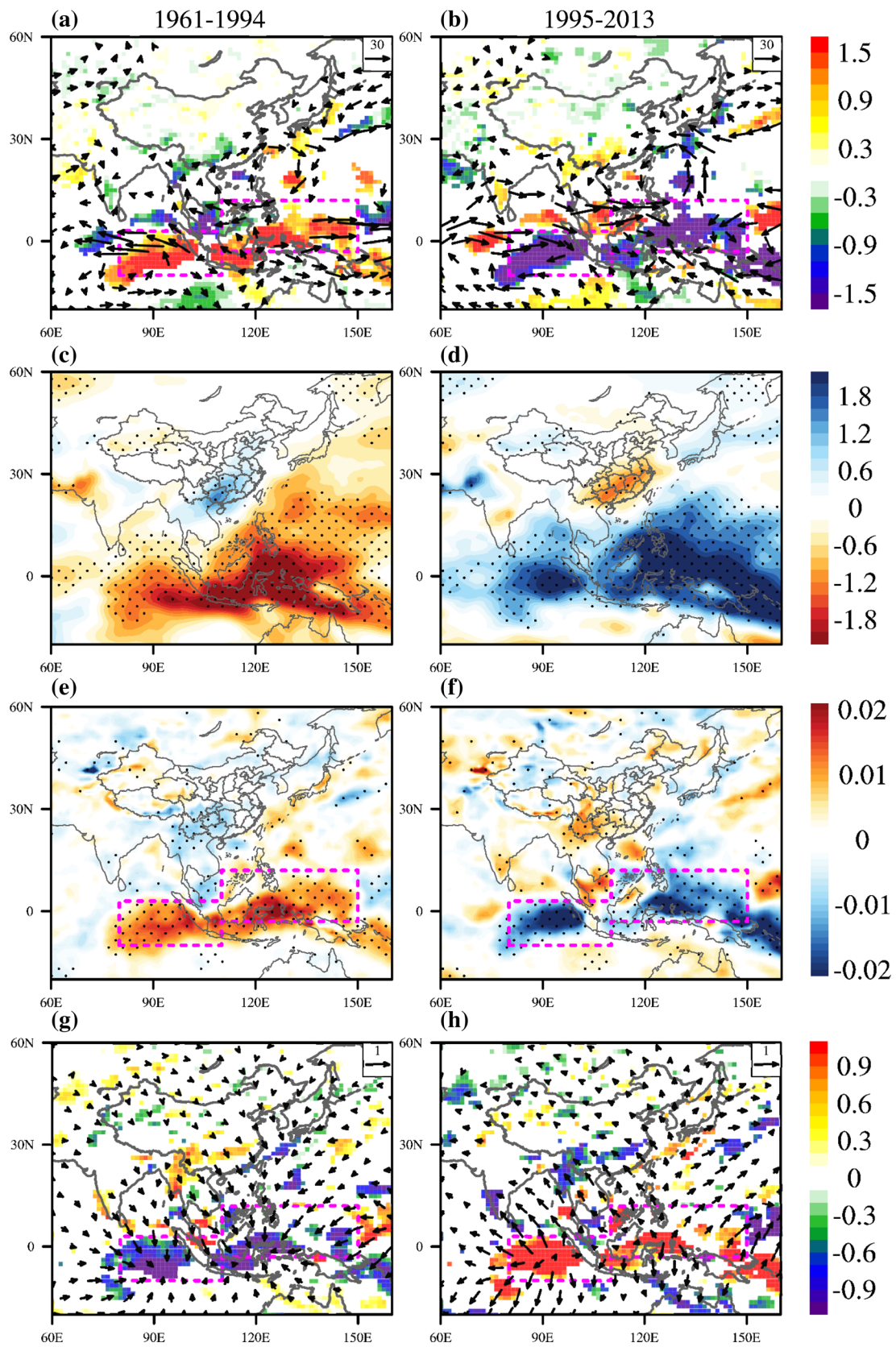


**Fig. 6** Composite anomalies for wet years 1961–1994 (left column) and dry years 1995–2013 (right column): **a, b** vertically integrated moisture flux (vectors, units:  $\text{kg s}^{-1} \text{m}^{-1}$ ) and divergence (shadings, units:  $10^{-5} \text{kg s}^{-1} \text{m}^{-2}$ ); **c, d** column precipitable water (shadings, units:  $\text{kg m}^{-2}$ ); **e, f** vertical velocity at 500 hPa (shadings, units:  $\text{Pa s}^{-1}$ ); **g, h** divergent wind (vectors, units:  $\text{m s}^{-1}$ ) and divergence (shadings, units:  $10^{-6} \text{s}^{-1}$ ) at 200 hPa. Only values significant at the 90% confidence level are plotted or stippled. The pink box denotes the domain of TWP

decades of 1995–2013 (right column), as the wet composites display roughly identical features except with opposite anomalies.

Regarding moisture transport anomalies (Fig. 6b), three features are noteworthy: first, an anomalous cyclone appears over the South China Sea, which is oriented against the climatological anti-cyclonic moisture flow and thus weakens the moisture supply from the tropical western Pacific; second, there tends to be a weakening of the poleward moisture flux from the Indian Ocean to SWC, as a result of a stronger westerly zonal flow setting up between  $5^{\circ}\text{S}$  and  $5^{\circ}\text{N}$  and converging over the maritime continent; third, the anomalous northwestward advection along the south flank of the Tibetan Plateau deflects moisture to the northern Arabian Sea, but away from the track ending up in SWC. All of these collectively reduce moisture fluxes from moisture sources to sinks in SWC and produce strong divergence in SWC. In response to the blocking of the penetration of moist flows originating from lower latitudes, as shown in Fig. 6d, SWC loses part of its precipitable water content, while abundant moisture stays over its source region. Figure 6f, h aim to provide a perspective on the vertical structure. There is anomalous ascent and upper-level divergence over the equatorial western Pacific and eastern Indian Oceans, with one branch of the outflow heading northward or northwestward and converging aloft over SWC. As a result, local compensating subsidence prevails SWC and prevents the formation of convection and rainfall. In short, the configuration of the three-dimensional atmospheric circulation well explains the recent dry decades in SWC. In contrast, during 1961 to 1994 labeled wet, the general pattern favors an intensification of moisture advection into SWC and the uplifting processes are intensified, so that more rainfall is expected (left column).

Further, taking a panoramic view of the circulation dynamics, more in-depth understanding is gained. First, the atmospheric structures between the latter and former decadal periods appear almost perfectly symmetrical, indicating the symmetry in the underlying physical mechanisms. Second, north of latitude  $28^{\circ}\text{N}$  in SWC, the atmospheric anomaly is considerably less pronounced than it is to the south, which follows a south–north gradient in the amount of local precipitation departures, as mirrored in Fig. 4. Third, mostly importantly, the tropical warm pool stands out as a probable origin of the teleconnection. Accordingly,

we define the tropical warm pool (TWP) as concatenating the tropical northwest Pacific sector (TNWP,  $3^{\circ}\text{S}$ – $12^{\circ}\text{N}$  and  $110^{\circ}\text{E}$ – $150^{\circ}\text{E}$ ) and the tropical east Indian Ocean sector (TEI,  $10^{\circ}\text{S}$ – $3^{\circ}\text{N}$  and  $80^{\circ}\text{E}$ – $110^{\circ}\text{E}$ ), as delineated by the dashed rectangle in Fig. 6.

To provide preliminary understanding of the relevance of TWP SST to precipitation in SWC, a correlation map between the global SST and the precipitation in SWC is shown in Fig. 7. It confirms the statistically significant coupling between SWC precipitation and TWP SST: warm TWP SST corresponds to below-average precipitation in SWC and vice versa. Contrasting the time series of SWC precipitation (bars) and TWP SST (pink line) in Fig. 8, a striking out-of-phase relation between them is prominent. SST in the TWP region exhibits a strong transition from a relatively cold period prior to the mid-1990s to a warm period afterward. Repeating the CUSUM test procedure with TWP SST, the precise date of the regime shift for TWP SST is 1994 (Fig. 3b). In addition, the SST in TNWP and TEI share identical temporal behaviors with that of the whole area. Consequently, the abrupt shift to drier conditions in 1994 for SWC exactly coincides with a positive decadal switch of TWP SST, which is believed to be the dominant driver.

### 3.3 Numerical experiments

How does TWP SST affect the large-scale circulation and precipitation in SWC? To understand the physical mechanism, two suites of numerical experiments are launched to explore the dynamical responses related to diabatic heating in TWP as well as to isolate the roles of the eastern sector TNWP and the western sector TEI. Prior to the implementation, an idealized elliptic patch of SST anomalies is constructed and then imposed on autumn SST climatology. This patch is defined as the multiplication of amplitude  $A$  and horizontal distribution function  $H(x, y)$ :

$$\text{SSTA} = A \cdot H(x, y)$$

$$H(x, y) = \begin{cases} 1 - \sqrt{\frac{(x-x_c)^2}{(\Delta x)^2} + \frac{(y-y_c)^2}{(\Delta y)^2}}, & \frac{(x-x_c)^2}{(\Delta x)^2} + \frac{(y-y_c)^2}{(\Delta y)^2} \leq 1, \\ 0 & \text{otherwise} \end{cases}$$

where  $x_c$  and  $y_c$  are the center longitude and latitude of the patch,  $\Delta x$  and  $\Delta y$  are the width of the patch in zonal and meridional extension. This formula creates a gradual decrease of SST anomalies when moving away from the center of the patch, while outside the ellipse the values are set to zero. In this study, Amplitude  $A$  is chosen to be either  $1^{\circ}\text{C}$  or  $-1^{\circ}\text{C}$ . Six forcing conditions are prepared: (a) TNWP SST increased by  $1^{\circ}\text{C}$  (amplitude  $A$ ), (b) TNWP SST decreased by  $1^{\circ}\text{C}$ , (c) TEI SST increased by  $1^{\circ}\text{C}$ ,

**Fig. 7** Correlation pattern between autumn precipitation for SWC and global SST, with statistically significant ( $P < 0.05$ ) correlations stippled

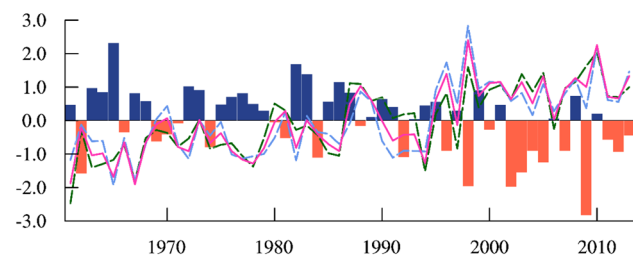
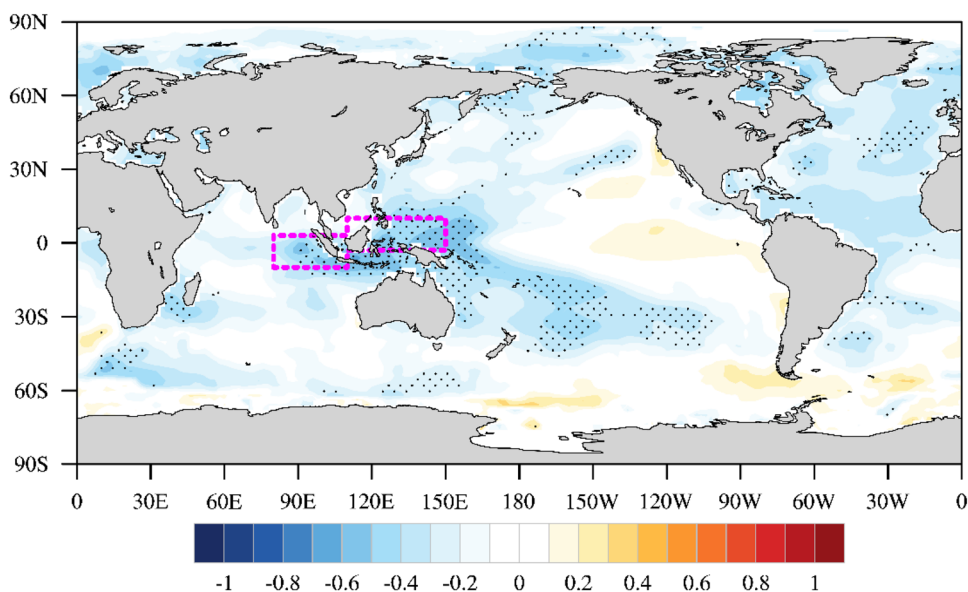


**Fig. 8** Anomalous time series of autumn precipitation in SWC (bars) and SST in TWP (pink solid line), TNWP (blue dashed line) and TEI (green dashed line)

(d) TEI SST decreased by  $1\text{ }^{\circ}\text{C}$ , (e) TWP (TNWP + TEI) SST increased by  $1\text{ }^{\circ}\text{C}$ , and (f) TWP (TNWP + TEI) SST decreased by  $1\text{ }^{\circ}\text{C}$ , as shown in Fig. 9.

LBM and CAM experiments are executed separately, but under the same forcing field. LBM is integrated for 50 days and the last 30-day average is approximated as the steady solution. Note that there is no control run for LBM. For the CAM simulations, the control experiment consists of 20 years of integrations forced with climatological SST, while warm and cold experiments are initialized on the first day of 10th year from control experiment and run for 10 years. The mean differences between control and perturbation experiments over the last 10 years are analyzed, in order to remove the internal variability of the model and highlight the SST-induced anomalous pattern.

Figure 10 shows the response of the horizontal wind at 700 hPa (vectors) and total water vapor (shadings) in moist LBM. Looking at the effect of TNWP forcing (the first row in Fig. 10), a classic Gill-type response (Gill 1980) in the troposphere emerges as the most notable feature. In the case

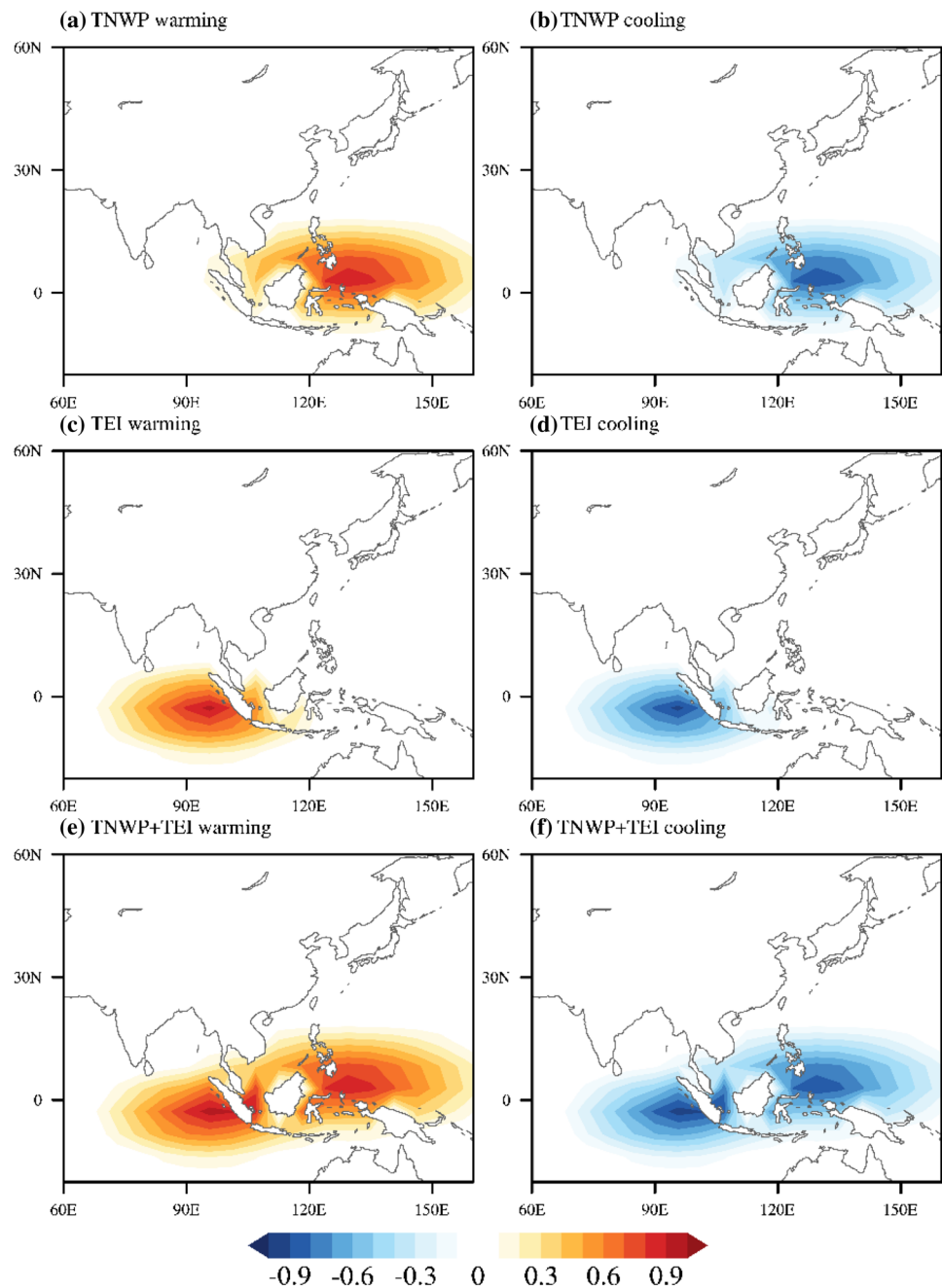
of the warm state (Fig. 10a), an anomalous cyclonic circulation to the northwest of the heat source interrupts the moisture supply from the equatorial western Pacific, and strong zonal wind to the west of the heating zone incurs a much smaller portion of the expected poleward transport to SWC. As a result, large volumes of water vapor are trapped in TNWP, whereas the moisture content drops significantly in SWC. In contrast, in the presence of the cold SST, a symmetrical response with an opposite sign is found, which favors water vapor escaping from the source region to SWC.

The second row of Fig. 10 reveals the influence of TEI. When warm SST anomalies are used (Fig. 10c), westerlies appear along the equator toward TEI and northwestward wind along the south flank of the Tibetan Plateau. The former promotes strengthened convergence in TEI, and the latter steers water vapor to the northern Arabian Sea, both of which lead to a decrease in precipitable water over SWC. In contrast, the cold SST sensitivity experiment (Fig. 10d) produces an opposite atmospheric pattern that is favorable for precipitation in SWC.

Figure 10e, f evaluate the joint effect of TNWP and TEI, reflecting that the thermal conditions in both sectors act in a synergistic fashion to generate climate anomalies in SWC. Most importantly, it is found that the TWP-induced patterns closely resemble the observed ones, highlighting that TWP alone constitutes a perfect oceanic scenario for inducing decadal change in the circulation pattern over East Asia and precipitation in SWC. In addition, the anomalous intensity is weaker in the north than in the south of SWC, in line with the observation as shown in Fig. 4.

As LBM is simple linear model, can the teleconnected patterns seen in LBM realizations be generated in the AGCM's climate? Figure 11 depicts the dynamical responses

**Fig. 9** SST anomaly patterns specified in the modeling experiments. **a** TNWP warming by 1 °C, **b** TNWP cooling by 1 °C, **c** TEI warming by 1 °C, **d** TEI cooling by 1 °C, **e** combination of TNWP and TEI warming, **f** combination of TNWP and TEI cooling

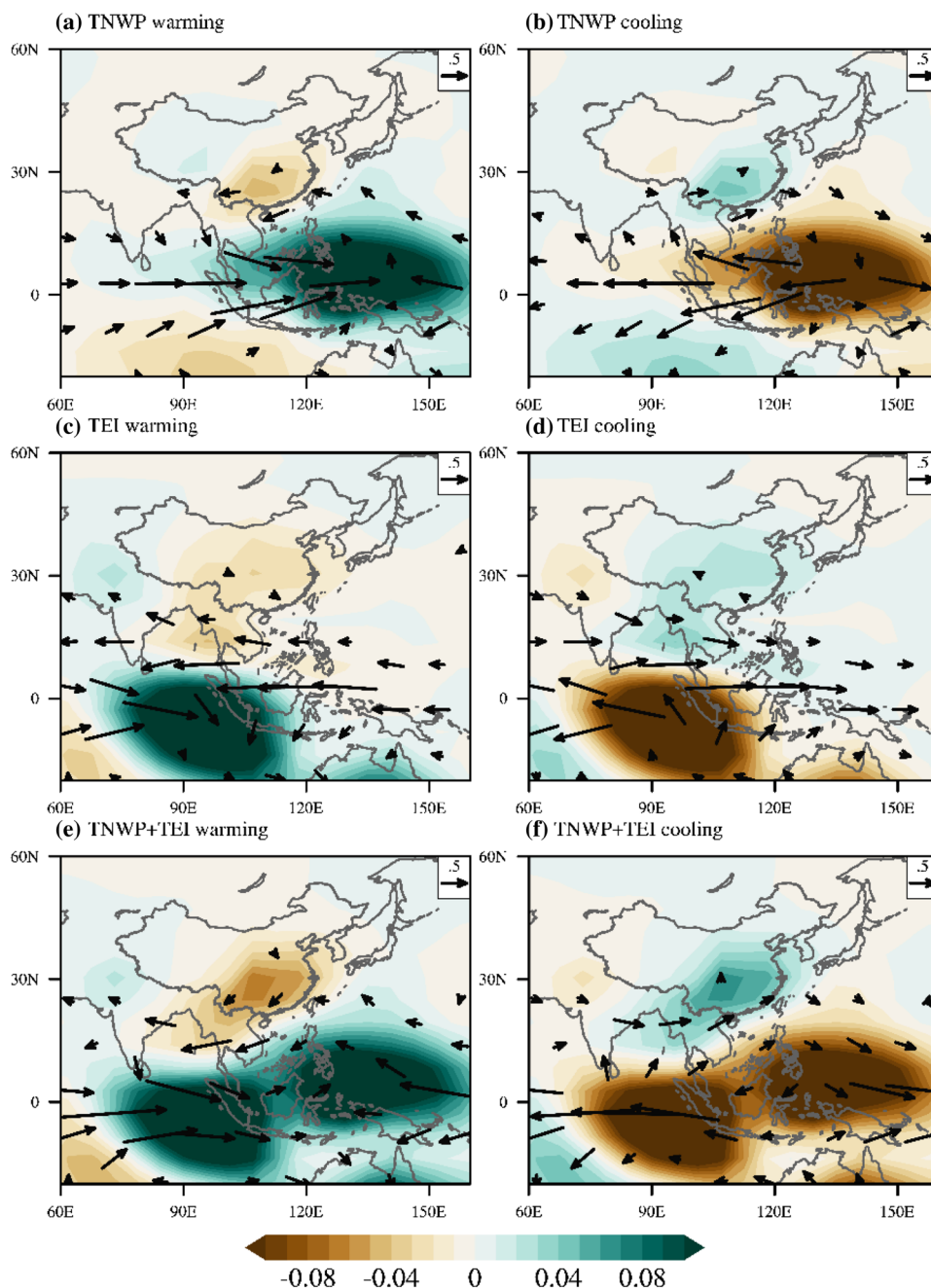


to SST anomalies prescribed in TWP alone based on the full non-linear model CAM. On the one side, a comparison of left and right columns in Fig. 11 indicates the symmetry in a spatial pattern related to warm and cold forcing, which is in common with the observation and LBM. On the other side, the horizontal and vertical structures formed in CAM experiments coincides well with those of observations. Here, we take the composite of warm experiment minus control for explanation (left column of Fig. 11). CAM reproduces the key features of horizontal moisture flux (Fig. 11a), including cyclone centered in the South China Sea, northward flow along the southern flank of the Tibetan Plateau

and intensified westerlies along the equator towards TWP region, accompanied with the moisture convergence over TWP sector and the divergence in SWC. Meanwhile, the vertical structure is also found to be remarkably similar between observation and CAM (Fig. 11c, e), as reflected by the meridional circulation in which the air rises over the warm SST region in TWP, flows toward the SWC region aloft and sinks there.

In brief summary, there is strong model-based evidence supporting the dominant role of TWP SST and the proposed physical mechanisms in regulating the decadal dry-wet variation in SWC.

**Fig. 10** The response of wind at 700 hPa (vectors, units:  $\text{m s}^{-1}$ ) and vertically integrated specific humidity (shadings, units:  $\text{kg kg}^{-1}$ ) in moist LBM, **a** TNWP warming, **b** TNWP cooling, **c** TEI warming, **d** TEI cooling, **e** both warming, and **d** both cooling



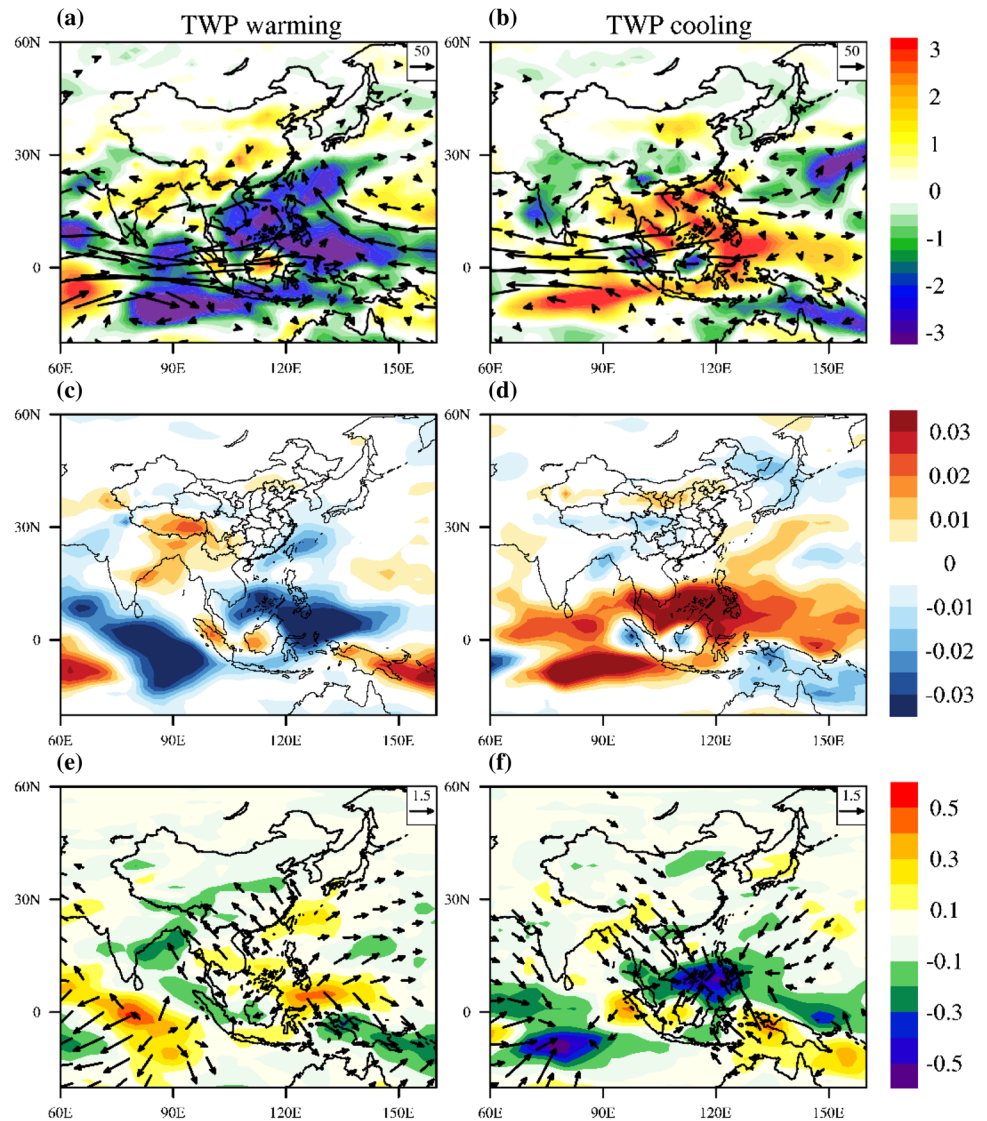
## 4 Conclusion

This study investigates the decadal dry-wet dynamics of autumn climate in SWC. The most remarkable feature related to SWC precipitation is the presence of one cycle of decadal variability, rather than any long-term climate trend. Based on the CUSUM test, the abrupt change from wet to dry occurred in 1994. To facilitate cause-and-effect analyses, the last 53 years are separated into two periods: wet decades (1961–1994) and dry decades (1995–2013). The composite of circulation and SST patterns before and after the 1994 climate shift suggests that the extratropical

response in the SWC region appears to be associated with remote TWP SST forcing. It is also interesting to note that there is a concurrent cold-to-warm phase switch of TWP SST in 1994, which probably gives rise to the wet-to-dry shift in SWC precipitation.

A mechanism is put forward to explain the role of TWP and its impact on decadal variability of SWC rainfall. The schematic diagram in Fig. 12 concisely depicts the major physical processes in response to diabatic forcing in TWP. Since TWP comprises the two sectors TNWP and TEI, the effects of TNWP and TEI are colored blue and green, respectively. Coupled with warm SST over the TNWP sector

**Fig. 11** Warm minus control (left column) and cold minus control (right column) differences in CAM: **a** vertically integrated moisture transport (vectors, units:  $\text{kg s}^{-1} \text{m}^{-1}$ ) and moisture divergence (shadings, units:  $10^{-5} \text{kg s}^{-1} \text{m}^{-2}$ ), **b** pressure vertical velocity at 500 hPa (shadings, units:  $\text{Pa s}^{-1}$ ), **c** divergent winds (vectors, units:  $\text{m s}^{-1}$ ) and divergence (shadings, units:  $10^{-5} \text{s}^{-1}$ ) at 200 hPa



(right panel in Fig. 12), there is an anomalous cyclone centered on the South China Sea and an enhanced westerly to the west of TNWP, which inhibit the moisture supply from the tropical Pacific and Indian Oceans, respectively. In parallel, warm SST over TEI intensifies the westerly to the west of TEI followed by less concurrent transfer of moisture to SWC, and generates a northwestward flow along the southern flank of the Tibetan Plateau, which steers the water vapor away from the SWC-oriented track. Meanwhile, the troposphere over SWC is capped by subsidence, which is jointly contributed by TNWP and TEI. All of these are conducive to a deficient moisture supply, divergence conditions, and suppressed convection in SWC, resulting in an overall paucity of rainfall during 1995–2013. In contrast, cold TWP SST tends to provide beneficial conditions for a wet SWC (left panel in Fig. 12), as the atmosphere in direct contact with TWP forcing exhibits a symmetrical response with respect to the sign of the SST anomalies.

Most importantly, the consistency between the observations and model results with SST forcing specified only in TWP verifies the primary influence of TWP SST on SWC precipitation at a decadal timescale. In addition, the magnitude of interdecadal change in SWC is not homogeneous throughout SWC but is characterized by a south-north gradient, due to stronger TWP SST-driven circulation in the southern SWC than in the northern SWC.

## 5 Discussion

The main idea of this study is that decadal variability of TWP SST exerts a major influence on the decadal behavior of autumn precipitation in SWC. Further, the obvious question arises: why does cold-to-warm shift happen in TWP sector?

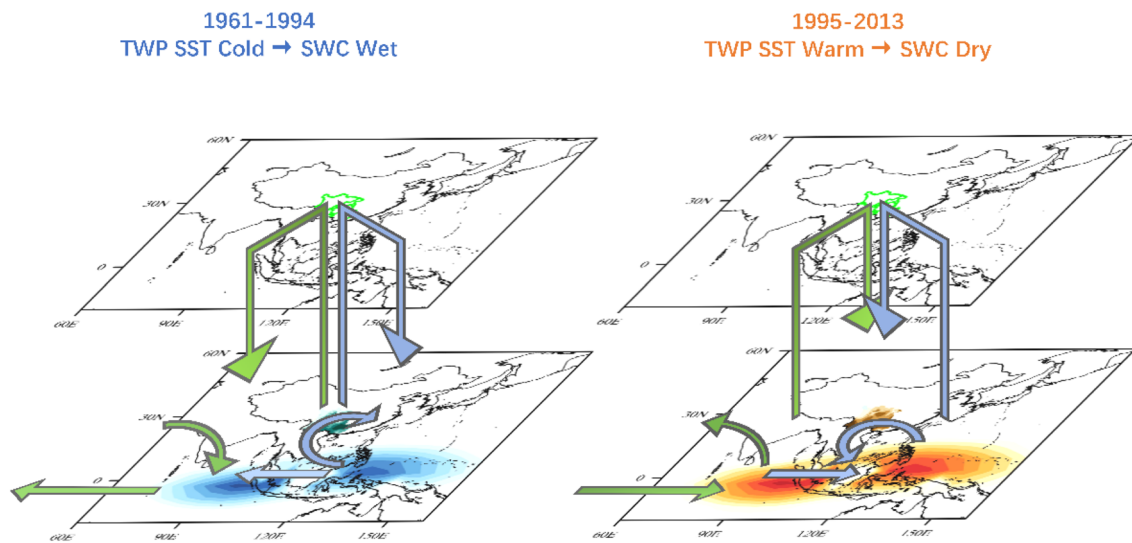


**Fig. 12** Schematic diagram of major atmospheric responses associated with cold (left panel) and warm (right panel) TWP SST anomalies. The direct effects arising from TNWP and TEI are denoted in blue and green, respectively

This shift may be part of long-term pattern of interdecadal oscillation in the climate of Pacific basin, which is known as interdecadal Pacific oscillation (IPO). The IPO emerges as a dominant mode of intrinsic decadal SST variability, and operates at a multi-decadal scale with phases lasting around 20–30 years (Power et al. 1999). The spatial pattern of IPO resembles a horseshoe, having SST anomalies of one sign in the central and eastern tropical Pacific surrounded by anomalies of opposite sign values in the northwest and southwest Pacific. Since 1990s, the IPO has switched to cold phase, coupled with strengthening of zonal SST gradient and accelerated trade wind in the equatorial Pacific Ocean. As a result, firstly, such changes drives additional heat into the western Pacific with concurrent cooling in the eastern Pacific (Maher et al. 2017). This explains the warming in TNWP region. Secondly, such changes result in an increase in the strength and subsequent heat transport of the Indonesian throughflow, which transports some of the additional heat from the western Pacific into the Indian Ocean (Maher et al. 2017). This offers the reason for the warming in TEI region. Last, also note that the rainfall-SST correlations to some extent manifest as a IPO-like pattern, as shown in Fig. 7. However, the correlation hardly exceeds the 5% significance level, except over the TWP. Thus, it can be inferred that IPO has indirect influence on SWC precipitation through its influence on TWP SST.

In the future, more research is needed to reveal other potential candidates that directly or indirectly contribute to drought in SWC, for example Atlantic multidecadal oscillation, greenhouse gas, aerosols, solar activities and etc.

**Acknowledgements** We thank the anonymous reviewers for their constructive comments and suggestions. I'm grateful to Dr. Chao He from Jinan University for his help in porting the LBM package to the machine architecture. Part of this work was conducted at City University of Hong Kong. This work was supported by the National Natural Science Foundation of China Grant nos. 41505069, 41425019, 41461144001, 41721004 and 41530425, public science and technology research funds projects of ocean Grant no. 201505013, the State Key Laboratory of Tropical Oceanography, South China Sea Institute of Oceanology, Chinese Academy of Sciences (Project no. LTO1707), and the Shenzhen Science and Technology Plan Grant no. JCYJ20160422090117011.

## References

- Barriopedro D, Gouveia CM, Trigo RM, Wang L (2012) The 2009/10 drought in China: possible causes and impacts on vegetation. *J Hydrometeorol* 13:1251–1267
- Chen W, Wang L, Xue Y, Sun S (2009) Variabilities of the spring river runoff system in East China and their relations to precipitation and sea surface temperature. *Int J Climatol* 29:1381–1394
- Chen J, Wu R, Wen Z (2012) Contribution of South China Sea tropical cyclones to southern China summer rainfall increase around 1993. *Adv Atmos Sci* 29(3):585–598
- Chen W, Feng J, Wu R (2013) Roles of ENSO and PDO in the link of the East Asian winter monsoon to the following summer monsoon. *J Clim* 26:622–635
- Chen J, Wen Z, Wu R, Chen Z (2015) Influences of northward propagating 25–90-day and quasi-biweekly oscillations on Eastern China summer rainfall. *Clim Dyn* 45:105–124
- Ding Y, Wang Z, Sun Y (2008) Inter-decadal variation of the summer precipitation in East China and its association with decreasing Asian summer monsoon. Part I: observed evidences. *Int J Climatol* 28:1139–1161
- Duan H, Wang S, Feng J (2014) Drought events and its influence in 2013 in China. *J Arid Meteorol* 32(2):310–316

- Feng J, Chen W, Tam C-Y, Zhou W (2011) Different impacts of El Niño and El Niño Modoki on China rainfall in the decaying phases. *Int J Climatol* 31:2091–2101
- Feng J, Wang L, Chen W (2014a) How does the East Asian summer monsoon behave in the decaying phase of El Niño during different PDO phases? *J Clim* 27:2682–2698
- Feng L, Li T, Yu W (2014b) Cause of severe droughts in Southwest China during 1951–2010. *Clim Dyn* 43(7–8):2033–2042
- Gill AE (1980) Some simple solutions for heat-induced tropical circulation. *Q J R Meteorol Soc* 106:447–462
- Harada Y, Kamahori H, Kobayashi C, Endo H, Kobayashi S, Ota Y, Onoda H, Onogi K, Miyaoka K, Takahashi K (2016) The JRA-55 reanalysis: representation of atmospheric circulation and climate variability. *J Meteor Soc Japan* 94:269–302
- Harris I, Jones PD, Osborn TJ, Lister DH (2014) Updated high-resolution grids of monthly climatic observations—the CRU TS3.10 Dataset. *Int J Climatol* 34(3):623–642
- Huang R, Liu Y, Wang L, Wang L (2012) Analyses of the causes of severe drought occurring in Southwest China from the fall of 2009 to the spring of 2010. *Chin J Atmos Sci* 36(3):443–457 (**Chinese**)
- Jia X, Ge J (2017) Interdecadal changes in the relationship between ENSO, EAWM, and the wintertime precipitation over China at the end of the twentieth century. *J Clim* 30(6):1923–1937
- Jia X, Lee J, Lin H, Alessandri A (2014) Interdecadal change in the Northern Hemisphere seasonal climate prediction skill: part I. The leading forced mode of atmospheric circulation. *Clim Dyn* 43:1595–1609
- Jia X, Lin H, Ge J (2015) The interdecadal change of ENSO impact on wintertime East Asian climate. *J Geophys Res* 120(23):918–911 (**935**)
- Kobayashi S, Ota Y, Harada Y, Ebata A, Moriya M, Onoda H, Onogi K, Kamahori H, Kobayashi C, Endo H, Miyaoka K, Takahashi K (2015) The JRA-55 Reanalysis: general specifications and basic characteristics. *J Meteor Soc Japan* 93:5–48
- Kuan CM, Hornik K (1995) The generalized fluctuation test: a unifying view. *Econometric Reviews* 14(2):135–161
- Li X, Zhou W (2016) Modulation of the interannual variation of the India-Burma Trough on the winter moisture supply over Southwest China. *Clim Dyn* 46(1–2):147–158
- Li Y, Xu H, Liu D (2009) Features of the extremely severe drought in the east of Southwest China and anomalies of atmospheric circulation in summer 2006. *Acta Meteorologica Sinica* 67:122–132
- Li X, Wen Z, Zhou W, Wang D (2012) Atmospheric water vapor transport associated with two decadal rainfall shifts over East China. *J Meteor Soc Japan* 90:587–602
- Liu P, Sui CH (2014) An observational analysis of the oceanic and atmospheric structure of global-scale multi-decadal variability. *Adv Atmos Sci* 31(2):316–330
- Maher N, England MH, Gupta AS, Spence P (2017) Role of Pacific trade winds in driving ocean temperatures during the recent slowdown and projections under a wind trend reversal. *Clim Dyn*. <https://doi.org/10.1007/s00382-017-3923-3>
- National Meteorological Information Center (2012) Assessment report of China's ground precipitation  $0.5^\circ \times 0.5^\circ$  gridded dataset (V2.0). National Meteorological Information Center, Beijing (**in Chinese**)
- Neale RB et al (2012) Description of the NCAR community atmosphere model (CAM 5.0). NCAR Tech. Note TN-486, p 274
- Peng J, Zhang Q, Bueh C (2007) On the characteristics and possible causes of a severe drought and heat wave in the Sichuan-Chongqing region in 2006. *Clim Environ Res* 12(3):464–474 (**Chinese**)
- Piao J, Chen W, Wei K, Liu Y, Graf HF, Ahn JB, Pogoreltsev A (2017) An abrupt rainfall decrease over the Asian inland plateau region around 1999 and the possible underlying mechanism. *Adv Atmos Sci* 34(4):456–468
- Ploberger W, Krämer W (1992) The CUSUM test with OLS residuals. *Econometrica* 60(2):271–285
- Power S, Casey T, Folland C, Colman A, Mehta V (1999) Inter-decadal modulation of the impact of ENSO on Australia. *Clim Dyn* 15(5):319–324
- Smith TM, Reynolds RW, Peterson TC, Lawrimore J (2008) Improvements NOAAs historical merged land–ocean Temp Analysis (1880–2006). *J Clim* 21:2283–2296
- Sun S et al (2016) Shift in potential evapotranspiration and its implications for dryness/wetness over Southwest China. *J Geophys Res Atmos* 121:9342–9355
- Sun S et al (2017) Attributing the changes in reference evapotranspiration in Southwestern China using a new separation method. *J Hydrometeorol* 18(3):777–798
- Tan H, Cai R, Chen J, Huang R (2017) Decadal winter drought in Southwest China since the late 1990s and its atmospheric teleconnection. *Int J Climatol* 37(1):455–467
- Vicente-Serrano SM, Beguería S, López-Moreno JI (2010) A multiscale drought index sensitive to global warming: the standardized precipitation evapotranspiration index. *J Clim* 23:1696–1718
- Wang L, Chen W (2012) Characteristics of multi-timescale variabilities of the drought over last 100 years in Southwest China. *Adv Meteorol Sci Technol* 2(4):21–26 (**Chinese**)
- Wang Z et al (2012) Analysis of climate anomaly and causation in summer 2011. *Meteorological Monthly* 38:448–455 (**Chinese**)
- Wang L, Chen W, Zhou W (2014) Assessment of future drought in Southwest China based on CMIP5 multimodel projections. *Adv Atmos Sci* 31(5):1035–1050
- Wang L, Chen W, Zhou W, Huang G (2015a) Drought in Southwest China: a review. *Atmos Oceanic Sci Lett* 8:339–344
- Wang L, Chen W, Zhou W, Huang G (2015b) Teleconnected influence of tropical Northwest Pacific sea surface temperature on interannual variability of autumn precipitation in Southwest China. *Clim Dyn* 45(9–10):2527–2539
- Wang L, Chen W, Zhou W, Huang G (2016) Understanding and detecting super extreme droughts in Southwest China through an integrated approach and index. *Q J R Meteorol Soc* 142:529–535
- Watanabe M, Jin FF (2003) A moist linear baroclinic model: coupled dynamical–convective response to El Niño. *J Clim* 16(8):1121–1139
- Wu R, Yang S, Wen Z, Huang G, Hu K (2012) Interdecadal change in the relationship of southern China summer rainfall with tropical Indo-Pacific SST. *Theor Appl Climatol* 108:119–133
- Yang J, Gong D, Wang W, Hu M, Mao R (2012) Extreme drought event of 2009/2010 over southwestern China. *Meteor Atmos Phys* 115:173–184
- Yuan F, Chen W, Zhou W (2012) Analysis of the role played by circulation in the persistent precipitation over South China in June 2010. *Adv Atmos Sci* 29(4):769–781
- Zeileis A, Kleiber C, Krämer W, Hornik K (2003) Testing and dating of structural changes in practice. *Comput Stat Data Anal* 44(1):109–123
- Zhang R, Wu B, Zhao P, Han J (2008) The decadal shift of the summer climate in the late 1980s over Eastern China and its possible causes. *Acta Meteorol Sin* 22:435–445
- Zhang C, Tang Q, Chen D, Li L, Liu X, Cui H (2017) Tracing changes in atmospheric moisture supply to the drying Southwest China. *Atmos Chem Phys* 17(17):10383–10393